www.czasopisma.pan.pl PAN www.journals.pan.pl

Arch. Metall. Mater. **66** (2021), 4, 1059-1066

DOI: 10.24425/amm.2021.136425

M.P. SARAVANAN[1*], K. MARIMUTHU[2], K. JAYABAL[3]

CHARACTERISTIC INVESTIGATION OF MACRO FIBER COMPOSITE STRUCTURE USING FE MODEL

In this investigation, the effective mechanical, coupling and dielectric properties of Macro-fiber-composites (MFCs) consisting of piezo-rod-element constituents are determined using representative volume element method combined with finite element analysis. Experiments are conducted on piezo-bar-element MFCs to understand the applicability of the proposed approach which would later be extended to composites with modified geometric pattern. The longitudinal strains with respect to static deflections of beam and forced displacements under varying electrical loads are measured for the MFCs, and compared with the numerical simulations. Based on the good agreement from the result comparisons of piezo-bar-element MFCs, the effective material properties of piezo-rod-element MFCs are numerically determined based on the RVE approach.

Keywords: Macro-fiber Composite, Finite-Element Model, Piezoelectric Composite, ANSYS, RVE Method

1. Introduction

Macro-Fiber-Composites (MFC), Active-Fiber-Composite (AFC), Piezoceramic alloys and Shape-Memory Alloy (SMA) are used for variety of applications including vibration and shape control, energy harvesting, aircraft deicing, and flight control. Piezoelectric material has several stages of development, from piezoelectric ceramic to Piezoelectric-fiber Composite (PFC) by Smart Material Corp and AFC by MIT to MFC by NASA Langley Research Center in 1999, for its electro-mechanical coupling, blocking force and response time. Piezoceramic is a particular substance which could apply an external stress voltage and conversely, creates stress [1]. It is a commonly used material for actuator, energy harvesting and sensor technology, and due to its quick response time, wide bandwidth, and ability to develop large forces. Piezoelectric materials are patched to versatile light-weight structures, thereby offering intrinsic sensing and actuating capabilities for intelligent structures [2]. The piezoelectric in AFCs have circular cross section fibers which have embedded with epoxy resins and contact with the flatted grid electrodes and composite structure associated with the alignment of PZT fibers [3].

The MFCs are flexible in order to be in compliance with curved, bend and torsion surfaces easily. The actuation force in MFC is larger than a PZT, since the effect of d_{33} mode dominates as actuation and the effect of d_{31} mode as elongator. In d_{31} type MFC, applied voltages are mutually perpendicular to PZT fiber direction and as a result, the transverse strain is obtained due to coupling of d_{31} constant. Similarly, d_{33} type MFC has fiber orientation along longitudinal direction in alignment with the macroscopic polling direction, and the longitudinal strain is obtained through d_{33} constant [4]. Various studies have been performed for MFC constituent properties using analytical and numerical approaches. The advantage of MFC remains in its high flexibility, high actuating force and increased strain output. Therefore, it is commonly used in sensing and actuating structures. The probability of determining identical, homogeneous properties of the constituent properties have been studied and an easy analytical mixing rules are extracted according to the Uniform-Field Method (UFM) [5].

Many researchers focused on determination of effective material properties and electromechanical coupling constant of MFC based on experimental and numerical probes due the difficulties on homogeneous response of MFC with smart structure. Yang Kuang [6] developed a PZT transducer model to evaluate properties of MFCs by experimental and numerical power-output method for energy harvester. Zhong Zhe Dong [7] described that the constitutive relations of bonded plate with MFC transducers

1 MOHAMED SATHAK AJ COLLEGE OF ENGINEERING, CHENNAI, INDIA
2 COIMBATORE INSTITUTE OF TECHNOLOGY, COIMBATORE, INDIA
3 INDIAN INSTITUTE OF INFORMATION TECHNOLOGY, DESIGN AND MANUFACTURING, KANCHEEPURAM, CHENNAI, INDIA

* Corresponding author: saravanan.design89@gmail.com

and developed MFC transducers to derive the direct effect of coupling as equivalent forces to the reverse effect of piezoelectric under electrical boundary conditions for energy harvesting and vibration suppression. Latalski [8] developed MFC transducers and studied for detecting delamination and crack propagation and structural-health monitoring with operating conditions like restraining of vibration. Khazaee [9] developed an FE Model for PZT beams and improved flexibility by modifying geometrical and material properties and analyzed to expand natural and modal frequency and output electric power by changing the fibers rotation, cross-section area in substrate and the layer of active piezoelectric in macro scales. Brett Williams [10] designed intelligent structures of elastic MFC actuator to predict the non-linear characteristics and effect of poisson ratio under boundary conditions of closed loop circuit by applied electric field using traditional method. Guimarães [11] proposed to design smart structures with MFCs using FEM and compared to validate hard piezoelectric ceramics displacement findings and controlled clamped beam for 1st Mode of Vibration.

Jose [12] discussed about kirchoff classical plate theory theory based on which developed was FE model based on this they developed FE Model for controlling of active thin laminated structures. The dynamic instability of nonlinear model of cross ply laminate cantilever plates with MFC using Zig-Zag theory was developed and expanded for novelty by Hao [13]. Zhang [14] developed smart structures for arbitrary fiber reinforcement angles using linear piezoelectric constitutive equations. Panda [15] presented FE model of simply supported smart functionally graded (FG) plates with thermal environment. They specified nonlinear thermo-electro-mechanical coupled finite element model based on the first order shear deformation theory and the Von Karman type geometric nonlinearity.

Akash Pandey [16-18] derived a non-linear analysis of cumulative-damage theory to determine the stiffness of MFC by varying thermo-mechanical conditions for studying the fatigue life cycle behavior of MFC (d_{33} & d_{31} type) actuation and to find the angle of piezoelectric fiber. Acosta [19] estimated pyroelectric coefficients of thermal expansion using theoretical and experimental observations of MFCs. Tan [20] developed a nonlinear electro elastic model of MFC actuator and experimentally validated for resonant natural frequencies of the first mode under minimum and maximum voltage levels. The electro-elastic properties of MFCs were calculated by formulation of mixed rule combination for properties of the RVE. Jiao [21] demonstrated a new mechanism to increase both longitudinal and transverse strains with variation of peak value at voltage bias and less frequency response.

A wide range of research is carried out based on the variation of fiber angle & fiber orientation of MFC using finite element analysis but not on the piezo fiber structure of the ma-

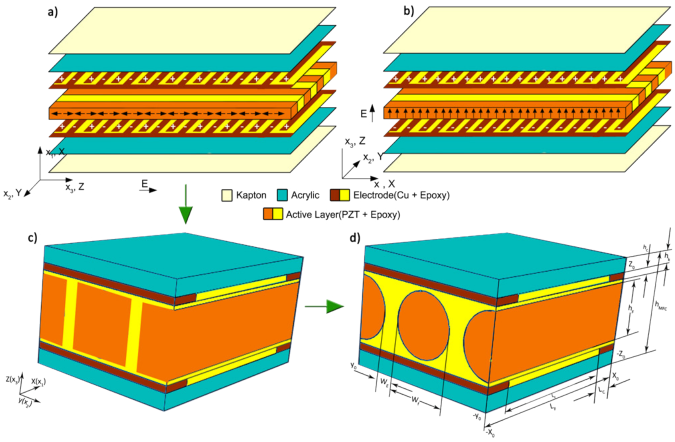

Fig. 1. Schematic diagram of a) longitudinal P1 type (d_{33} mode) and b) Transverse P2 type (d_{31} mode) type of MFCs c) Representative volume element (RVE) of piezo fiber bar for MFC d) Representative volume element (RVE) of piezo fiber rod for MFC

TABLE 1

Dimensions of RVE piezo fiber bar of MFC actuator (Manufacturer data)

Parameter	Symbol	Value (μm)	Parameter	Symbol	Value (μm)	Parameter	Symbol	Value (μm)
Width of the Fiber bar	W_f	185	Height of the Copper	h_C	18	Length of the epoxy	L_E	380
Height of the Fiber bar	h_f	185	Length of the Copper	L_C	80	Width of the epoxy	W_E	28.35
Length of the Fiber bar	L_f	420	Height of the MFC	h_{MFC}	260	Height of the Kapton	h_k	40

TABLE 2

Dimensions of RVE piezo fiber rod of MFC actuator (Data assumed and used)

Parameter	Symbol	Value (μm)	Parameter	Symbol	Value (μm)	Parameter	Symbol	Value (μm)
Diameter of the Fiber rod	W_f	185	Height of the Copper	h_C	18	Length of the epoxy	L_E	380
Length of the Fiber rod	L_f	420	Length of the Copper	L_C	80	Width of the epoxy	W_E	28.35
Height of the Kapton	h_k	40	Height of the MFC	h_{MFC}	260			

terial. We propose a model to develop and simulate integrated monolithic thin layered piezo fiber rod type cylindrical element structure of d_{31} & d_{33} mode using RVE method. The MFC layer consists of monotonic piezo fiber material, copper electrodes and epoxy matrix as homogenized elastic materials like composite material arrangement as shown in Fig. 1(a) and Fig. 1(b). This model is validated for actuation of MFCs by comparing the effective electromechanical properties between piezo fiber bar (Fig. 1(c), Tab. 1) and piezo fiber rod (Fig. 1(d), Tab. 2) RVE after applying electric potential to the fiber. This comparison is not only determined by analytical method but also simulated method, and this will help to find strain output matched with mean error and induced strain energy at free conditions. The proposed models of piezo fiber rod are analyzed with the effective properties by taking into account the fiber-volume-fraction (FVF) of circular orientation form of the constituent and its location. Subsequently, the material properties obtained from the model are compared with the manufacturer data and found in good agreement.

2. Finite element model formulation

NASA developed MFCs with an active-piezoelectric composite that have an active layer, two electrodes of rectangular piezo fibers and copper rods bonded with epoxy resin matrix, two acrylic and kapton layers that characterizes the behavior of actuation/sensing respectively. The material properties of piezo fibers and non-piezo constituents given in Tab. 3 and Tab. 4. have more advantages as compared to the constituents of other piezo-composites used in smart structures. MFCs consist of two types depending upon the applied poling direction and electric field, namely P_1 type as longitudinal (d_{33} mode as elongator) and P_2 type as transverse (d_{31} mode as contractor), direction of PZT fiber phase.

TABLE 3

Material properties for piezo fiber in MFCs

Sl. No.	Engineering Constants	Symbol	Unit	PZT 5A [21,62,63]
1.	Young's Modulus	E_1 (Ex)	GPa	45.21
		E_2 (Ey)	GPa	12.39
		E_3 (Ez)	GPa	40.44
2.	Shear's Modulus	G_{12} (G_{xy})	GPa	6.03
		G_{23} (G_{yz})	GPa	6.668
		G_{13} (G_{zx})	GPa	17.01
3.	Poisson's ratio	V_{12} (V_{xy})	—	0.39
		V_{23} (V_{yz})	—	0.17
		V_{13} (V_{xz})	—	0.44
4.	Density	ρ	kg/m^3	7600

TABLE 4

Material properties for non-piezoelectric layer materials in MFCs

Sl. No.	Engineering Constants	Symbol	Unit	Kapton	Copper	Epoxy
1.	Young's Modulus	E	GPa	3.1	110	3.3
2.	Poisson's ratio	V	—	0.42	0.35	0.34
3.	Density	ρ	kg/m^3	1420	8700	1300
4.	Dielectric Relative Constant	ε_T	—	3.4 ε_0	5 ε_0	4.25 ε_0

FEM based numerical analysis were conducted to compare the geometric properties of composite constituents. Steiger [22,23] developed a FE model of unit-cell approach to determine 1-3 Piezocomposite properties on RVE. In the proposed work, the model is extended to investigate the cylindrical structure of piezo fiber rod element and compared with the previous cuboid structure of piezo fiber bar element highlighting the improvement in results.

RVE is an approach in a fiber composite of periodic AFC Structure, where formulations of FE-Model are made. The computational costs and time are significantly minimized by using unit cell method. The schematic representation of RVE of piezo fiber bar for MFCs is shown in Fig. 1(c). The number of active nodes is increased to predict the elastic constants, displacements in between symmetric surfaces and the strain along the direction of poling with shear and normal strains remaining zero along the opposite directions by applying periodic boundary-conditions (PBC). To ensure short circuit condition, the electric potential variation between the symmetrical surfaces is maintained at zero. The constitutive relationship and macroscopic values of induced stress-strain, dielectric permittivity, electric displacement and coupling coefficients are calculated using volume-average technique.

The constitutive relations of orthotropic MFC actuators are provided below. Therefore, the general form of effective elastic stiffness properties of MFC actuator [25] can be represented as,

$$\{S\} = \left[s^E\right]\{T\} + [d]\{E\} \tag{1}$$

where, $[s^E]$ refers to the elastic constants, $[d]$ to the piezoelectric constants, E to the electric field, and T the mechanical stress of MFC actuator.

$$\begin{Bmatrix} S_1 \\ S_2 \\ S_3 \\ S_4 \\ S_5 \\ S_6 \end{Bmatrix} = \begin{bmatrix} s_{11}^E & s_{12}^E & s_{13}^E & 0 & 0 & 0 \\ s_{12}^E & s_{22}^E & s_{13}^E & 0 & 0 & 0 \\ s_{13}^E & s_{12}^E & s_{33}^E & 0 & 0 & 0 \\ 0 & 0 & 0 & s_{44}^E & 0 & 0 \\ 0 & 0 & 0 & 0 & s_{55}^E & 0 \\ 0 & 0 & 0 & 0 & 0 & s_{66}^E \end{bmatrix} \times$$

$$\times \begin{Bmatrix} T_1 \\ T_2 \\ T_3 \\ T_4 \\ T_5 \\ T_6 \end{Bmatrix} + \begin{bmatrix} 0 & 0 & d_{13} \\ 0 & 0 & d_{13} \\ 0 & 0 & d_{33} \\ 0 & d_{13} & 0 \\ d_{13} & 0 & 0 \\ 0 & 0 & 0 \end{bmatrix} \begin{Bmatrix} E_1 \\ E_2 \\ E_3 \end{Bmatrix} \tag{2}$$

2.1. Boundary conditions for RVE Macroscopic element

The specification of RVE surface boundary conditions are presented in Tab. 5, wherein, $x_0 = ½ \times l$, $y_0 = ½ (w_E + w_f)$, and $z_0 = ½ \times h_{MFC}$.

TABLE 5

Periodic-boundary conditions for RVE

Sl. No.	Parameters of Material	RV Element Surface	Direction of Testing force
1.	E_{11}	$x = \pm x_0$	(±1, 0, 0)
2.	E_{12}	$y = \pm y_0$	(0, ±1, 0)
3.	E_{23}	$z = \pm z_0$	(0, 0, ±1)
4.	G_{12}	$x = \pm x_0$	(0, ±1, 0)
		$y = \pm y_0$	(±1, 0, 0)
5.	G_{23}	$y = \pm y_0$	(0, 0, ±1)
		$z = \pm z_0$	(0, ±1, 0)
6.	G_{13}	$x = \pm x_0$	(0, 0, ±1)
		$z = \pm z_0$	(±1, 0, 0)

2.2. Averaging of effective piezoelectric and elastic properties and its state quantities

Average stresses based on volume of element:

$$T'_{ij} = \frac{1}{v}\int_v^0 T_{ij} \cdot dv \tag{3}$$

Average strains based on volume of element:

$$S'_{ij} = \frac{1}{v}\int_v^0 S_{ij} \cdot dv \tag{4}$$

The effective Young's moduli:

$$E_{ij} = \frac{T'_{ii}}{S'_{ii}} \tag{5}$$

$$G_{ij} = \frac{T'_{ij}}{2S'_{ij}} \tag{6}$$

$$\upsilon_{ij} = \frac{-S'_{ii}}{S'_{jj}} \tag{7}$$

$$d_{3i} = \frac{S'_{ii}}{V_0} \cdot h_{MFC} \tag{8}$$

where, v represents the volume of RVE, V_0 the applied voltage, d_{3i} the piezoelectric moduli, T'_{ii}, T'_{ij} and T'_{jj} the average stresses in v, S'_{ii}, S'_{ij} and S'_{jj} the average strains in v, E_{ij} the effective Young's moduli, G_{ij} the effective shear moduli, υ_{ij} the Poisson's ratio of MFC actuator and can be calculated with respect to i – 1,2,3,…6, j – 1,2,3,…6 are number of interdigitate order of the element by symmetric layers of piezoelectric fiber with parallel electrode plates [26].

3. Experimental Setup

In this experiment, the cantilever beam of Aluminium plate unimorph patch with MFCs as Evaluation kit, whose dimensions are given in Tab. 6, were placed at x-distance (x = 20 mm) from the fixed end [27] as shown in Fig. 2. The mode of d_{33} (M8528-P_1) and d_{31} (M8528-P_2) Type MFCs were brought under pure electrical potential voltage maintained within ranges from –500 V to +500 V, and –60 V to +60 V to study the experimental actuation responses. A motor-generator combination was used to induce the cyclic sinusoidal waveform for a given input signal of voltage and frequency to high-voltage amplifier. The high voltage which was about ten times higher than the original voltage was generated and applied to the MFC. The observed data of beam displacement, transverse and longitudinal strains were measured by using Laser-Displacement-Sensor (LDS). All experimental output signals from the LDS were recorded and measured though analog input module and cDAQ (NI9223) card Kit using NI LabVIEW software. The entire experimental setup was fixed over the anti-vibrational table for absorbing the external and environmental vibrations. The photograph of experimental setup is presented in Fig. 3.

TABLE 6

Dimensions of Aluminium cantilever beam patched with MFC

Parameter	Symbol	Value (mm)	Parameter	Symbol	Value (mm)
Width of the MFC	W_{MFC}	28	Width of the Beam	W	35
Height of the MFC	H_{MFC}	0.3	Height of the Beam	H	0.3
Length of the MFC	L_{MFC}	260	Length of the Beam	L	300

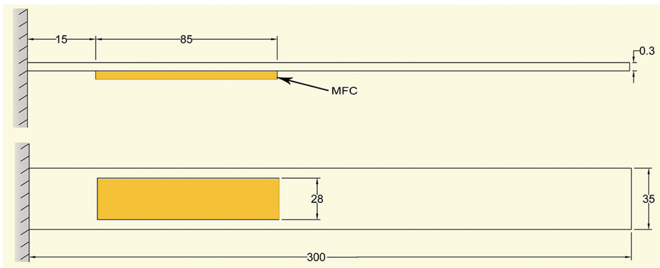

Fig. 2. Schematic diagram of Aluminum cantilever beam unimorph patched with MFC

4. Result and discussions

The influence of geometric and material properties of MFC constituents on the effective material properties of MFC is analyzed numerically. It is learnt that only a few finite element models are available for homogenization of all active layers recorded in literature for d_{33} and d_{31} type MFCs.

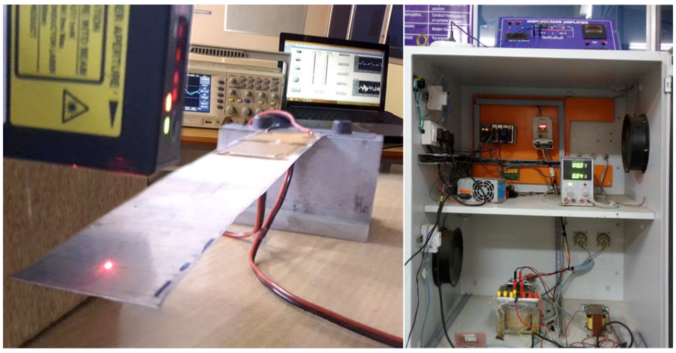

Fig. 3. Experimental setup of cantilever beam with MFC and High-Voltage Amplifier

4.1. Experimental result

An experimental corroboration is conducted to determine induced longitudinal strains on the beam with MFCs (d_{33} and d_{31} type) under various applied electric field as shown in Fig. 4 and Fig. 5. The observation data are used to estimate the volume fraction of electrode as non-active layer (copper and epoxy).

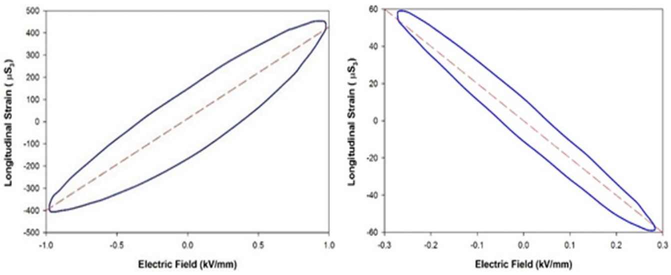

Fig. 4. Induced longitudinal strain distribution in MFCs (P1 and P2 Type) due to applied electric field

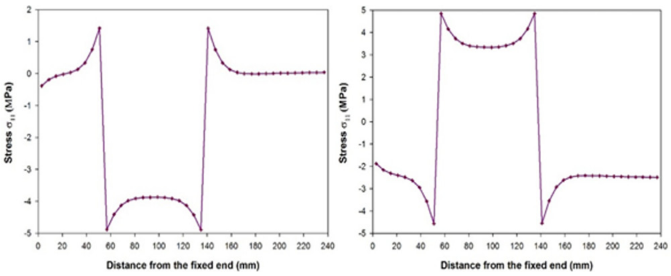

Fig. 5. Stress distribution on MFCs (P1 Type) with respect to distance from the fixed end

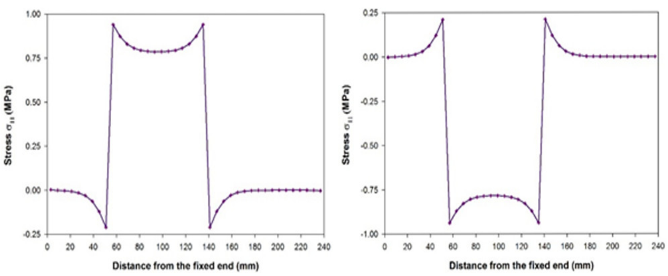

Fig. 6. Stress distribution on MFC11s (P2 Type) with respect to distance from the fixed end

Therefore, the proposed model is evaluated with the experimental observations in terms of effective material properties. Further, the structural analysis of cantilever beam with patched MFCs are carried-out with Kirchhoff plate theory and compared with FE model to calculate the variation of stress along beam thickness of 0.3 mm as shown in Fig. 6. Subsequently, the three invariants of principal stresses are analyzed based on the displacements of beam and the type of MFCs.

4.2. Numerical validation of active layer using RVE

A RVE integrated numerical FE model is analyzed for understanding the effective-coupling and piezoelectric constants for both types of MFCs using ANSYS with Piezo and MEMS module. Using Eq. 1 to 8, the material properties are calculated and fed into RVE to obtain the effective material properties for the FE model by applying electric field. In order to have a detailed study on the effective properties of fiber volume-fraction of PZT fiber (PZT 5A), the epoxy matrix along with fiber are considered as active layers. In the analysis of MFCs, the active layer (PZT fiber and epoxy) and electrode layers are connected parallel. The coupling constants are predicted by applying the PBC along the direction of displacement, while constraining the displacement in the other directions and maintaining the initial potential difference across the copper electrodes as zero.

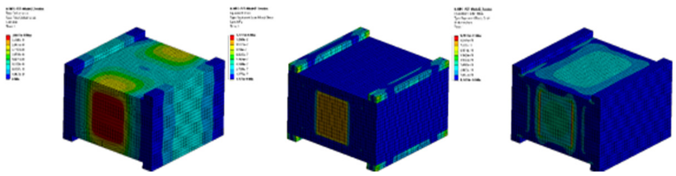

Fig. 7. Electric displacement, induced stress and strain distributions for applied electrical charges in RVE (piezo-fiber-bar) of MFC (P1 Type) d_{33} mode

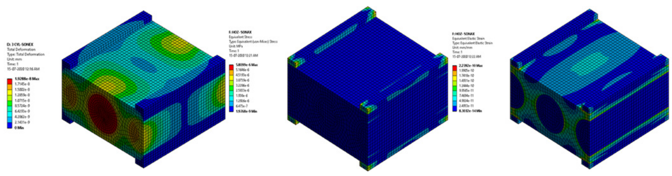

Fig. 8. Electric displacement, induced stress and strain distributions for applied electrical charges in RVE (piezo-fiber-rod) of MFC (P1 Type) d_{33} mode

In d_{33} type, the estimate indicates a non-linear variation of the coupling constants and dielectric constants as fiber fraction length increases as shown in Fig. 9. Since the epoxy matrix is passive in nature to the applied electric field, a minimum number of dipoles are available in lower fractions of the fiber length, resulting in minimum piezoelectric constants. At greater volume-fractions, the fiber supremacy increases, resulting in increased coupling constants.

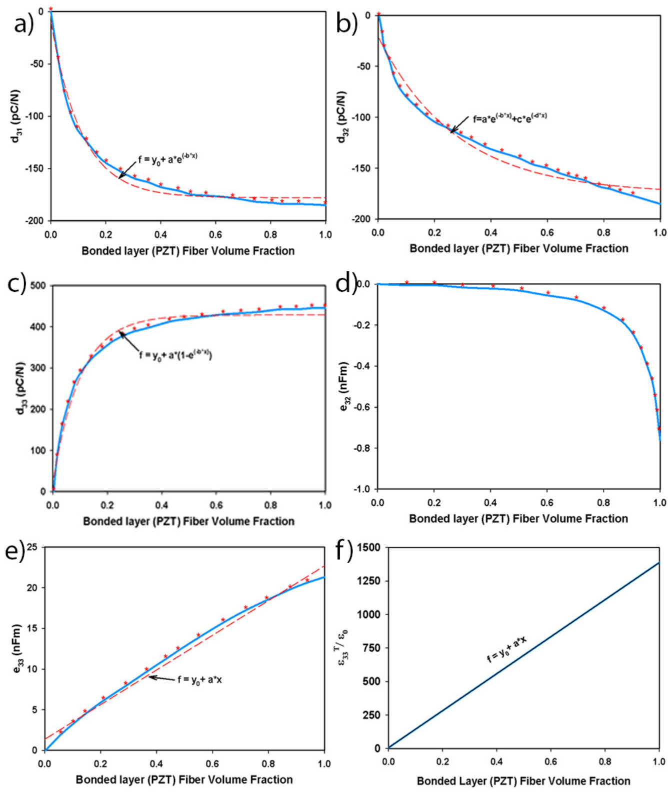

Fig. 9. Variation of effective coupling constants and dielectric constants of active layer of d_{33} type MFC

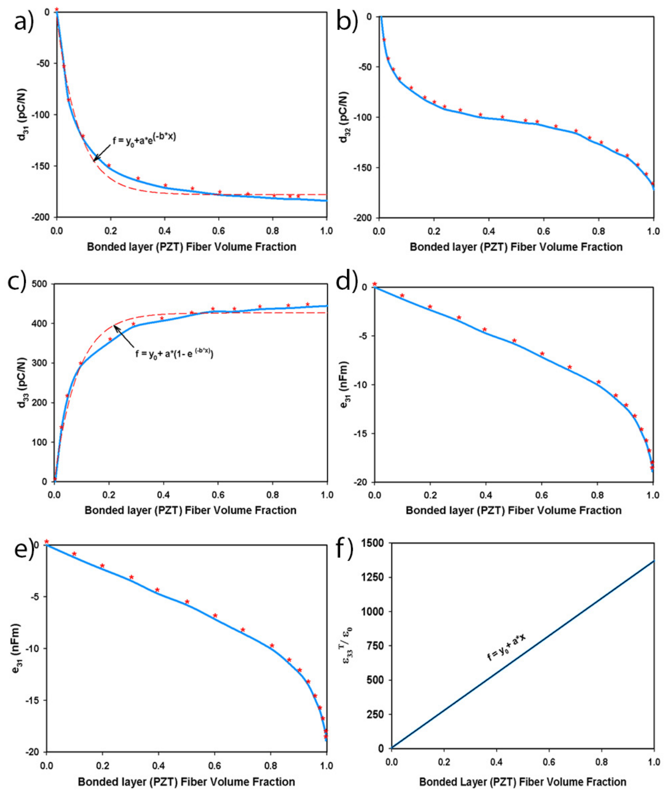

Fig. 12. Variations of effective coupling constants and dielectric constants of active layer of d_{31} type MFC

In d_{31} type, a non-linear variation of coupling constants (d_{31}, d_{32} and d_{33}) of the active layer is estimated. The estimate indicates variations of piezoelectric constants and dielectric permittivity as fiber volume fraction increases as seen in Fig. 12. At lower volume-fraction of piezo-fiber, as other phases are passive, only a minimal active material is available for overall response of MFC. Higher volume-fractions of piezo-fiber contribute to higher coupling constants, thereby, the MFC behavior changes accordingly. Fig. 15 shows the deflection of beam with

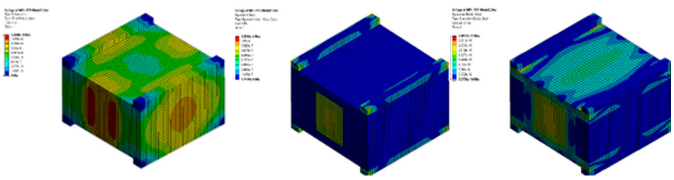

Fig. 10. Electric displacement, induced stress and strain distributions for applied electrical charges in RVE (piezo-fiber-bar) of MFC (P2 Type) d_{31} mode

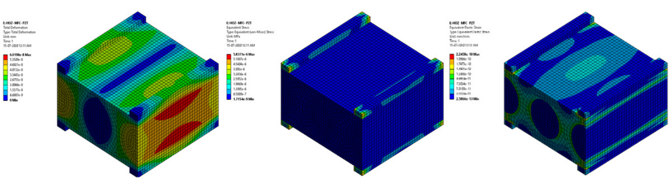

Fig. 11. Electric displacement, induced stress and strain distribution for applied electrical charges in RVE (piezo-fiber-rod) of MFC (P2 Type) d_{31} mode

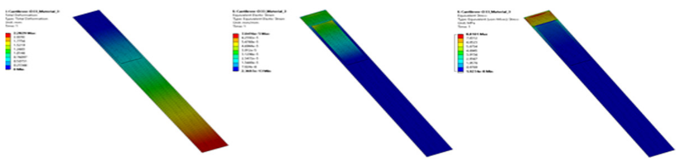

Fig. 13. FE analysis for mechanical behavior of cantilever beam with unimorph d_{33} mode MFC in terms of deflection, stress and strain, for various materials under applied electric Field

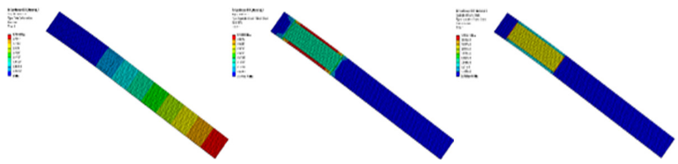

Fig. 14. FE analysis for mechanical behavior of cantilever beam with unimorph d_{31} mode MFC in terms of deflection, stress and strain, for various materials under applied electric Field

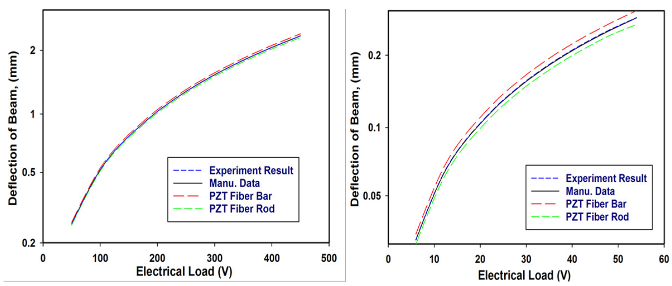

Fig. 15. Deflection of cantilever beam bonded with MFCs (P1 and P2 Type) due to electrical Potential load

TABLE 7

Comparison of material properties of MFCs with Manufacturers datasheet

Sl. No.	Engineering Constants	Symbol	Unit	From Manufacturer data [21]		RVE – piezo fibre bar [18,22,23,24,25]		RVE – piezo fibre rod (Obtained from proposed Model)	
				d_{33}	d_{31}	d_{33}	d_{31}	d_{33}	d_{31}
1.	Young's Modulus	E_1 (E_x)	GPa	29.4	30.336	30.41	32.58	26.86	27.42
		E_2 (E_y)	GPa	15.2	15.857	14.52	15.33	14.01	15.32
		E_3 (E_z)	GPa	—	—	9.12	9.37	8.63	9.15
2.	Shear's Modulus	G_{12} (G_{xy})	GPa	5.79	5.515	4.32	5.26	4.11	5.06
		G_{23} (G_{yz})	GPa	6.06	5.515	2.06	2.47	2.02	2.25
		G_{13} (G_{zx})	GPa	—	—	2.19	2.76	2.24	2.49
3.	Poisson's ratio	V_{12} (V_{xy})	—	0.42	0.310	0.286	0.313	0.324	0.307
		V_{23} (V_{yz})	—	0.31	0.160	0.214	0.147	0.289	0.132
		V_{13} (V_{xz})	—	—	—	0.327	0.405	0.316	0.383

respect to applied electric potential load and frequency obtained from the experimental observations, and compared with the FE simulations (Fig. 13 and 14) for both MFCs. Thereafter, the forced displacement, induced stress and strain are determined and compared with the experimental observations in Tab. 7 to validate the material properties with the Manufacturers' datasheet.

TABLE 8

Material Properties of Aluminium & Epoxy for cantilever beam [20]

Sl. No.	Engineering Constants	Symbol	Unit	Aluminium	Epoxy
1.	Young's Modulus	E	GPa	69	3.3
2.	Poisson's ratio	V	—	0.334	0.34
3.	Density	ρ	kg/m^3	2712	1300

5. Conclusions

In this work, a laminated thin-layered smart composite structure patched with d_{31} and d_{33} mode MFCs with piezo-bar-elements was considered as a cantilever beam, and their experimental responses on application of applied electric fields were observed. A representative volume element approach was used to determine the effective material properties of the MFCs, and provided as input to the finite element model of the composites. The responses obtained from the finite element analysis were compared with the experimental observations of piezo-bar-element MFCs in order to validate the developed approach. As the comparisons were found in good agreement, the approach was then extended to predict the mechanical, coupling and dielectric material properties of piezo-rod-element MFCs. It was observed from the numerical simulations, that the modified geometric pattern of piezo-fiber marginally improves the flexible behavior of the composites.

Acknowledgment

The authors acknowledge the funding support from AICTE, New Delhi under Research Proposal Scheme, for High-Voltage Amplifier Setup. The authors also acknowledge the experimental facility provided at Advanced Manufacturing Technology lab by Coimbatore Institute of Technology, Coimbatore, India.

REFERENCES

[1] R.J. Prazenica, D. Kim, H. Moncayo, B. Azizi, M. Chan, Design, Characterization, and Testing of Macro-Fiber Composite Actuators for Integration on a Fixed-Wing UAV, Proc. of SPIE **9057**, 905715-2 (2014).

[2] J.R. Farmer, A comparison of power harvesting techniques and related energy storage issues, Master of Science Thesis, Virginia Polytechnic Institute and State University, May (2017).

[3] J. Schröck, T. Meurer, A. Kugi, Control of a flexible beam actuated by macro-fiber composite patches: II. Hysteresis and creep compensation, experimental results, Smart Mater. Struct. **20**, 015016 (2011).

[4] R.B. Williams, Nonlinear Mechanical and Actuation Characterization of Piezoceramic Fiber Composites, PhD Thesis, Virginia Polytechnic Institute and State University, March (2004).

[5] S. Ju, C.H. Ji, Indirect Impact based Piezoelectric Energy Harvester for Low Frequency Vibration, IEEE Transd., USA, 978-1-4799-8955-3, June 21-25 (2015).

[6] Y. Kuang, M. Zhu, Evaluation and validation of equivalent properties of macro fibre composites for piezoelectric transducer modelling, Compos. Part B-Eng. **158**, 189-197 (2019).

[7] Z. Dong, C. Faria, B.P. luymers, M. Hromčí, M. Šebek, W. Desmet, Structure-preserving low-order modeling approach of laminated composite plates integrated with macro-fiber composite transducers for dynamic application, Compos. Struct. **208**, 287-297 (2019).

[8] J. Latalski, Modelling of Macro fiber composite piezoelectric active elements in abaqus system, E. I Niezawodnosc-Main. and Relia., December (2011).

[9] M. Khazaee, A. Rezaniakolaie, L. Rosendahl, A broadband macro-fiber-composite piezoelectric energy harvester for higher energy conversion from practical wideband vibrations, Nano Energy **76**, 104978 (2020).

[10] R.B. Williams, D.J. Inman, Nonlinear Tensile and Shear Behavior of Macro Fiber Composite Actuators, J. Compos. Mater. **38** (2004).

[11] C.S. Guimarães, V.P. Budinger, F.L.S. Bussamra, J.A. Hernandes, Structural Shape Control using Macro Fiber Composite Piezoelectric Sensors and Actuators, Comput. Mech., Argentina, 8263-8279, 15-18 (2010).

[12] Jose M. Simoes Moita, Isidoro F.P. Correia, Cristovao M. Mota Soares, Carlos A. Mota Soares, Active control of adaptive laminated structures with bonded piezoelectric sensors and actuators, CompuStruct. **82**, 1349-1358 (2004).

[13] Y.X. Hao, K.F. Zhao, W. Zhang, S.W. Yang, Nonlinear dynamics and dynamic instability of smart structural cross-ply laminated cantilever plates with MFC layer using zigzag theory, Appl. Mathematical Mod (2019).
DOI: https://doi.org/j.apm.2019.10.056 (in press).

[14] Shun-Qi Zhang, Ya-Xi Li, Rudiger Schmidt, Modeling and simulation of macro-fiber composite layered smart structures, Comp. Struct **51**, (2015).

[15] Satyajit Panda, M.C. Ray, Nonlinear finite element analysis of functionally graded plates integrated with patches of piezoelectric fiber reinforced composite, Finite Elements in Analysis and Design **44**, 493-504 (2008)

[16] A. Pandey, A. Arockiarajan, An experimental and theoretical fatigue study on macro fiber composite (MFC) under thermo-mechanical loadings, Eur. J. Mech. A-Solid (2017).
DOI: https://doi.org/10.1016/j.euromechsol.2017.06.005

[17] A. Pandey, A. Arockiarajan, Fatigue study on the sensor performance of Macro Fiber Composite (MFC): Theoretical and experimental approach, Compos. Struct. **174**, 301-318 (2017).

[18] A. Pandey, A. Arockiarajan, Performance studies on Macro Fiber composite(MFC) under thermal condition using Kirchhoff and Mindlin plate theories, Int. J. Mech. Sci. (2017).
DOI: https://doi.org/10.1016/j.ijmecsci.2017.06.034

[19] K.L. Acosta, S. Srivastava, W.K. Wilkie, D.J. Inman, Primary and secondary pyroelectric effects in macro-fiber composites, Compos. Part B-Eng. **177**, 107275 (2019).

[20] D. Tan, P. Yavarow, A. Erturk, Nonlinear elastodynamics of piezoelectric macro-fiber composites with interdigitated electrodes for resonant actuation, Compos. Struct. (2017).
DOI: https://doi.org/10.1016/j.compstruct.2017.12.056

[21] Q. Jiao, Ji. Hongli, Q. Jinhao, The synergism of peak to peak value, frequency and superimposed DC bias voltage on electric-field-induced strain of PZT based-macro fiber composites, Ceram. Int. **45**, 22067-22077 (2019).

[22] K. Steiger, P. Mokrý, Finite element analysis of the macro fiber composite actuator: macroscopic elastic and piezoelectric properties and active control thereof by means of negative capacitance shunt circuit, IOP Publishing, Smart Mater. Struct. **24**, 025026 (2015).

[23] S. Sreenivasa Prasath, A. Arockiarajan, Effective electromechanical response of macro-fiber composite (MFC): Analytical and numerical models, Int. J. Mech. Sci. **77**, 98-106 (2013).

[24] Z. Abas, H.S. Kim, L. Zhai, J. Kim, Finite element analysis of vibration driven electro-active paper energy harvester with experimental verification, Adv. Mech. Eng. **22**, 1-9 (2015).

[25] IEEE Standards on Piezoelectricity, ANSI/IEEE Standard, The Institute of Electrical and Electronic Engineers, New York, 1988.

[26] S. Sreenivasa Prasath, A. Arockiarajan, Analytical, numerical and experimental electromechanical predictions of the effective properties of macro-fiber composite (MFC), Sensor. Actuat. A-Phy. **214**, 31-44 (2014).

[27] M.P. Saravanan, K. Marimuthu, P. Sivaprakasam, Modeling and analysis of dynamic structure with macro fiber composite for energy harvesting, Mater. Today-Proc. (2020).
DOI: https://doi.org/10.1016/j.matpr.2020.05.390, 2214-7853 (in press).

[28] Smart-Material Corporation, MFC Datasheet,
https://www.smart-material.com/Datasheets.html

[29] A. Pandey, A. Arockiarajan, Actuation performance of macro-fiber composite (MFC): Modeling and experimental studies, Sensor. Actuat. A-Phy. **248**, 114-129 (2016).